FERMILAB-PUB-20-093-TD
ACCEPTED
10.1109/TASC.2020.2974706

HEAT TREATMENT STUDIES OF Nb_3Sn WIRES FOR SUPERCONDUCTING PLANAR UNDULATORS

E. Barzi, D. Turrioni, Y. Ivanyushenkov, M. Kasa, I. Kesgin, and A.V. Zlobin

***Abstract*—A project aiming to fabricate a full-length 2.8-m long Nb_3Sn superconducting undulator for the storage ring was started last year at the ANL APS. These Nb_3Sn undulators operate at a maximum magnetic field on the conductor of about 5 T. To address instabilities at this field, two Nb_3Sn wires with small subelement size were used. Specifically, Restacked Rod Processed wires of 0.6 mm in diameter and with 144 and 150 superconducting subelements respectively, over 169 total. The equivalent subelement diameter, D_S, of these wires is ~35 μm. At these small D_S values, the critical current density is known to deteriorate, and the Residual Resistivity Ratio is very sensitive to heat treatment. A delicate balance has therefore to be found to obtain parameters within operation specifications. In this paper we show performance results from different heat treatments.**

***Index Terms*— Undulator magnet, critical current density, Nb_3Sn strand, Residual Resistivity Ratio.**

I. INTRODUCTION

SUPERCONDUCTING undulators (SCUs) made of Nb-Ti have been successfully designed and installed at the ANL Advanced Photon Source (APS) since 2013 [1]-[3]. They increased the brightness of X-ray beams in the high energy spectrum by an order of magnitude with respect to permanent magnets. More recently, an ANL APS group and the FNAL High Field Magnet team paired forces to develop a double undulator of 2.8 m total length made of Nb_3Sn, to be installed in the APS storage ring. In addition to a larger temperature margin than Nb-Ti, Nb_3Sn undulators are expected to increase the magnetic field in the electron beam aperture by up to 50%. Such increase of the field reduces the number of required spatial periods while increasing the energy range of the first harmonic of the emitted radiation. A reduction in length of free electron lasers would deliver consistent cost savings. For synchrotron light sources, an increase in the energy range and brightness intensity of the photon beam would generate invaluable performance improvements and expand research capabilities. If successful, a Nb_3Sn APS undulator would be the first operating insertion device based on Nb_3Sn.

Of the three phases of this project, the first one was successfully completed [4], [5]. Six short Nb_3Sn models of 4.5 periods length and 10 poles (Small Magnet Models) were designed, fabricated and tested. They were used to optimize the winding, heat treatment (HT) and assembly procedure and solve any technical problems that arose during these processes. In addition, this phase was critical to obtain and prove reproducibility in performance. A second phase will see scale-up of the short models to 0.5 m long magnets (Intermediate Magnet Models), to ensure magnetic field quality on-axis, and adequate quench protection. The third phase will be used to scale-up to the actual 1.4 m long magnets to be installed in the APS storage ring.

For the very first undulator short model SMM1, a standard HT, which is typically used for Rutherford cables made of Internal Tin Nb_3Sn wires, was chosen [6]. An example is given in Table II in the "STUDY" last row. For subsequent short models, which were wound out of wires with smaller superconducting (SC) filaments, or subelements, the HT schedule was changed by decreasing the temperature and increasing the time of the second step. This was done to account for Nausite formation, at the lower temperature stages of the HT, which in case of small filaments reduces critical current density J_c [7]. The latter HT was successful, in that it indeed increased the expected J_c. However, analyses showed that for a maximum field on the conductor of about 5 T and for state-of-the-art values of J_c, the transverse size of the SC subelements has to be 36 μm or less to ensure stability to flux jumps [8]. It was therefore important to verify that the selected HT not only provided the best J_cs, but also the desired stability behavior in the lower field regions, where the undulator load line intersects the superconductor critical or quench current curve.

The same two Restacked Rod Processed (RRP®) wires of 0.6 mm in diameter that were used in the winding of the short magnet models following the first were studied when subjected to the standard HT, shown in the "STUDY" row of Table II. These wires had 144 and 150 SC subelements respectively, over 169 total subelements. Critical current I_c and Residual Resistivity Ratio *RRR* were measured and compared with those of the witness samples used for short magnet models SMM4, SMM5, and SMM6.

II. STRAND AND TEST PARAMETERS

A. Strand Description

Table I shows parameters of the RRP wires of 0.6 mm size produced by Bruker-OST (BOST) and used in the undulator

The work supported by Fermi Research Alliance, LLC, under contract Nos. DE-AC02-07CH11359 and DE-AC02-06CH11357 with the U.S. Department of Energy.

E. Barzi, D. Turrioni and A.V. Zlobin are with the Fermi National Accelerator Laboratory (Fermilab), Batavia, IL 60510 USA (e-mail: barzi@fnal.gov).

Y. Ivanyushenkov, M. Kasa and I. Kesgin are with Advanced Photon Source, Argonne National Laboratory, Lemont, IL 60439 USA.

short magnet models SMM2, SMM3, SMM4, SMM5 and SMM6, as well as in the intermediate magnet model IMM1. The wire denoted as RRP1 has a 150/169 stack design, and RRP2 has a 144/169 design. This notation represents the number of SC bundles in the billet matrix over the total number of SC and Cu restacks. For instance, the 150/169 wire has 150 SC bundles within a layout of 169 restacks. All these wires also have extra Cu between the subelements. The RRP wire cross sections are shown in Fig. 1.

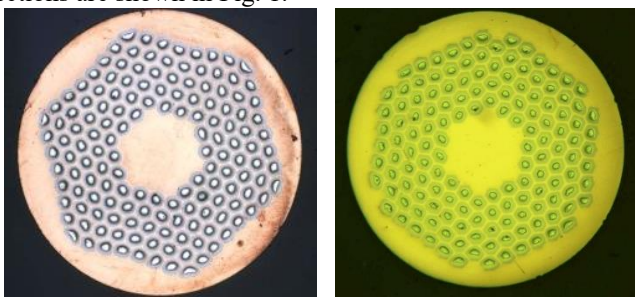

Fig. 1. Cross sections of 150/169 (left) and 144/169 (right) RRP wires used in undulator short magnet models.

In Table I, D_S is the equivalent subelement diameter calculated in the approximation that the subelements be round instead of hexagonal. The final HT steps shown in Table I are those used by BOST to obtain the data in the Table.

TABLE I
STRAND PARAMETERS – BOST DATA

Strand ID	RRP1	RRP2
Stack design	150/169	144/169
Ternary element	Ti	Ti
Production year	2018	2019
Diameter *d*, mm	0.601	0.602
I_c (4.2K, 12 T), A	345 ± 2	336 ± 3*
J_c (4.2K, 12 T), A/mm^2	2,426 ± 7	2,499 ± 23*
D_S, μm	35	35
Twist pitch, mm	14.5 ± 0.4	16
Cu fraction λ, %	50 ± 0.1	52.4
RRR	93 ± 11	143 ± 11
Final HT step	650ºC/50 h	640ºC/50 h

*Extrapolated value.

B. Heat Treatments

Together with each undulator small model, four samples of the round wire that had been used in the coils were included in the reaction oven for HT in inert Argon. Six samples of round wire were used for the undulator intermediate model and the dummy coil. In addition to monitoring the accuracy and homogeneity of the reaction temperatures with calibrated and ungrounded K-type thermocouples, these so-called witness samples are then characterized for transport current and other properties such as *RRR*, to ensure quality of the coil reaction. Nb_3Sn wires were wound on grooved cylindrical Ti-alloy (Ti-6Al-4V) barrels, and held in place by two removable Ti-alloy end rings. Fig. 2 shows short magnet model SMM5 in its reaction fixture prior to reaction at FNAL. In the picture, the locations of the four cylindrical barrels holding the witness samples are also shown with respect to the magnet. In Table II the HT parameters actually obtained as measured by the thermocouples are shown for small magnet models SMM4, SMM5, SMM6, for intermediate magnet model IMM1, for a slightly modified HT using a dummy coil and, under "STUDY", for several RRP1 and RRP2 round samples heat treated with the standard HT. All the thermal cycles shown in Table, aside for intermediate magnet model IMM1 and the dummy coil, were performed in the same 3-zone controlled tube furnace with a 12" long temperature homogeneity volume. IMM1 and the dummy coil were heat treated in a 2 m long oven with much larger homogeneity volume.

TABLE II
HEAT TREATMENT SCHEDULES

	STEP 1		STEP 2		STEP 3	
COIL	Temp, ºC	Time, hr	Temp, ºC	Time, hr	Temp, ºC	Time, hr
SMM4	209 ± 1	48	369 ± 2	104	651 ± 1	50
SMM5	210 ± 1	48	369 ± 2	104	650 ± 1	50
SMM6	210 ± 1	48	371 ± 1	104	650 ± 1	50
IMM1*	211 ± 1	48	370 ± 1	104	650 ± 2	50
DUMMY*	210 ± 2	48	370 ± 3	104	650 ± 3	40
STUDY	210 ± 2	48	401 ± 1	48	649 ± 1	50

*Heat treated in larger oven.

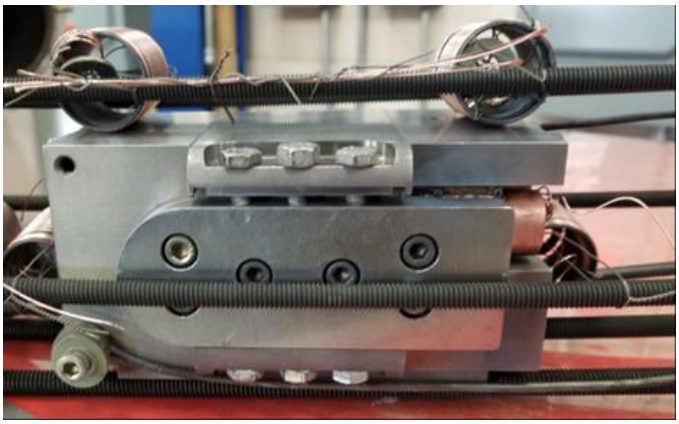

Fig. 2. SMM5 in reaction fixture prior to reaction at FNAL. The locations of the four cylindrical barrels holding the witness samples are also shown.

C. Strand Tests

After HT, the Ti-alloy end rings are removed from the Ti-alloy barrels and replaced by Cu rings. Voltage-current (*V-I*) characteristics are measured in boiling He at 4.2 K, in a transverse magnetic field. In standard strand I_c measurements, three pairs of voltage taps are used. Two pairs are placed along the center of the spiral sample 50 cm and 75 cm apart, and one pair at the Cu leads to be used for quench protection. The I_c was determined from the *V-I* curve using the electrical field criterion of 0.1 μV/cm. Typical I_c measurement uncertainties are within ±1% at 4.2 K and 12 T.

III. RESULTS

A. Critical Current and Magnet Short Sample Limits

The I_c of the round wire is a key starting point for magnet design. Small magnet models SMM4 and SMM5 used RRP1, small magnet model SMM6 and intermediate magnet model IMM1 used RRP2 (see also Table III).

TABLE III
SUMMARY OF RESULTS

COIL	WIRE	Ave. I_c(12 T), A	Ave. B_{c20}, T	Ave. RRR	SSL, A
SMM4	RRP1	332 ± 2	26.7 ± 0.1	87 ± 2	1220
SMM5	RRP1	336 ± 1	26.7 ± 0.0	73 ± 2	1231
SMM6	RRP2	324 ± 6	26.9 ± 0.3	54 ± 2	1132
IMM1	RRP2	360 ± 7	27.8 ± 0.1	81 ± 5	1206
DUMMY	RRP2	358 ± 2	27.6 ± 0.1	96 ± 6	1205
STUDY	RRP1	288 ±6	25.1 ± 0.3	92 ± 5	1183*
	RRP2	279 ± 4	25.3 ± 0.2	55 ± 3	1114

*Interpolated value.

The results of I_c measurements vs. magnetic field for the RRP1 witness samples from SMM4 and SMM5 were compared with those from the standard HT in Figs. 3 and 4 respectively. Of the four witness samples used for each coil, the best and the least performing in I_c are plotted. In average, as shown in Table III, the I_c(12 T,4.2 K) of both SMM4 and SMM5 witness samples (RRP1) is 16% larger than in the standard HT. Nevertheless, their stability is better in the low field region (see below).

The results of I_c measurements vs. magnetic field for the RRP2 witness samples from SMM6 were compared with those from the standard HT in Fig. 5. Of the four witness samples used for SMM6, the best and the least performing in I_c are plotted. As shown in Table III, the average I_c(12 T, 4.2 K) of the witness samples is 16% larger than in the standard heat treatment also for SMM6, which was made with RRP2. Nevertheless, also in this case their stability behavior is better in the low field region. A more detailed discussion follows in the next paragraphs.

The $I_c(B)$ dependences provided the short sample limit (*SSL*) values for SMM4, SMM5, and SMM6, as well as nominal *SSL* values from the Study, as shown in Table III. It is to be noted that a 16% reduction in I_c (12T) corresponds to just a 2-4% difference in the short sample limit values.

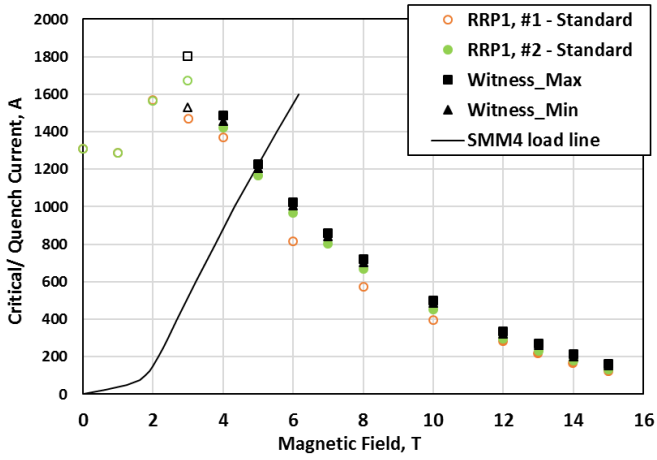

Fig. 3. Comparison of I_c (4.2 K) measurements (closed markers) vs. magnetic field for the RRP1 witness samples from SMM4 with those from the standard heat treatment. Of the four witness samples used, the best and the least performing in I_c are plotted. Open markers indicate early quenches without any *V-I* transition. The maximum field load line of SMM4 is also shown.

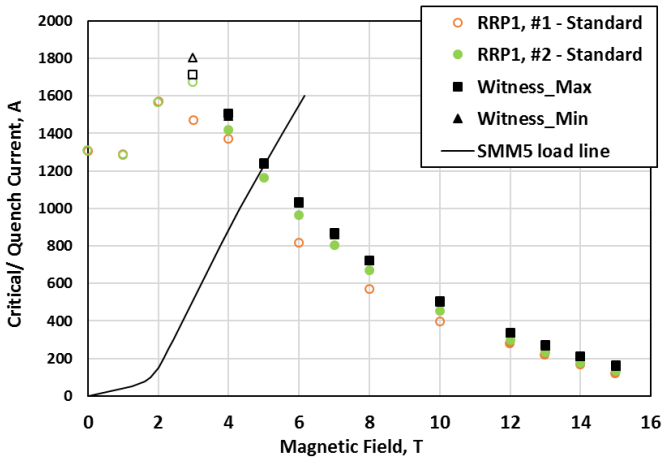

Fig. 4. Comparison of I_c (4.2 K) measurements (closed markers) vs. magnetic field for the RRP1 witness samples from SMM5 with those from the standard heat treatment. Of the four witness samples used, the best and the least performing in I_c are plotted. Open markers indicate early quenches without any *V-I* transition. The maximum field load line of SMM5 is also shown.

Looking at Figs. 3, 4 and 5, for all three small magnet models the unstable transport behavior of the witness samples starts at fields below the intersecting field of about 5 T with their critical current curve. This is not the case for the RRP1 wire under standard HT, which is unstable also above 5 T. In addition, the transport current of the RRP2 wire under standard HT dips dangerously below its nominal short sample limit (*SSL*) of 1114 A (see also Table III) in the *I-B* area encompassed within (i.e. at the left of) the magnet load line. Were this to be representative of a magnet behavior, the current in the magnet would never exceed the minimum value of 964 A shown in Fig. 5. This might be a reason for the past failure of Nb_3Sn undulators [9-13].

Finally, in Fig. 6 the results of I_c measurements vs. magnetic field were compared between the most unstable RRP2 from the standard HT and the most unstable of the witness samples from IMM1. The closed markers indicate the I_c(4.2K)

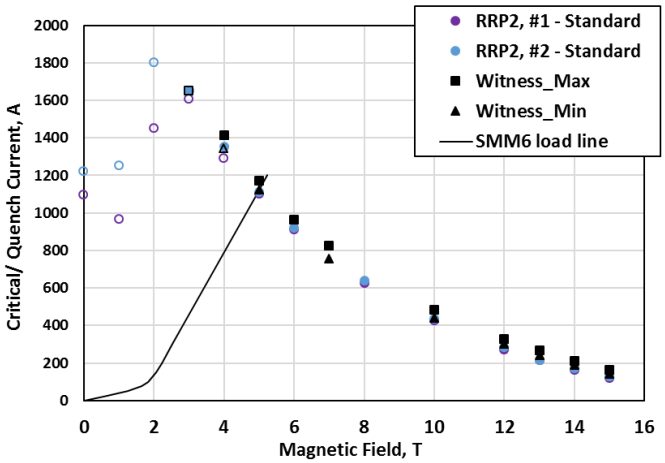

Fig. 5. Comparison of I_c (4.2 K) measurements (closed markers) vs. magnetic field for the RRP2 witness samples from SMM6 with those from the standard heat treatment. Of the four witness samples used, the best and the least performing in I_c are plotted. Open markers indicate early quenches without any *V-I* transition. The maximum field load line of SMM6 is also shown.

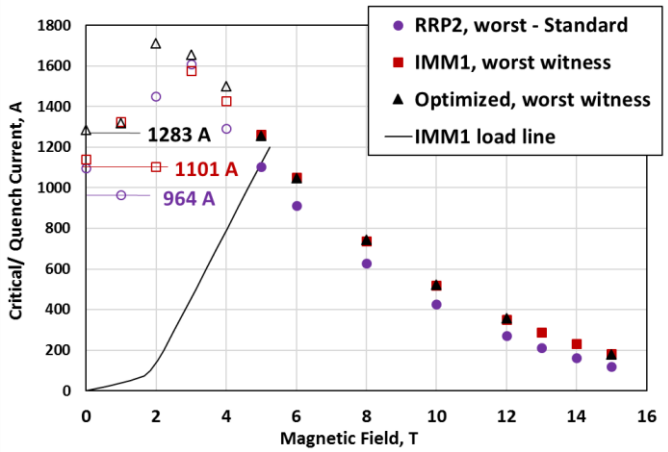

Fig. 6. Comparison of I_c *(4.2 K)* measurements (closed markers) vs. magnetic field between the most unstable RRP2 from the standard heat treatment, the most unstable of the witness samples from IMM1, and the most unstable from a further optimized heat treatment using a dummy coil. Open markers indicate early quenches without any *V-I* transition. An approximation of the maximum field load line of IMM1 is also shown.

obtained from a smooth *V-I* transition from the superconducting to the normal state, open markers indicate early quenches without any *V-I* transition. Perhaps thanks to the larger temperature homogeneity volume provided by the 2 m long oven used, or to a larger Argon flow rate, the average J_c*(12 T, 4.2 K)* of the IMM1 witness samples was 2675 A/mm^2, i.e. more than 10% larger than for SMM6, with a theoretical *SSL* of 1206 A (see Table III). However, the transport current of the most unstable IMM1 witness sample in Fig. 6 has a local minimum of 1101 A in the *I-B* area encompassed within (i.e. at the left of) the magnet load line. This is below IMM1 *SSL*, which will never therefore be achieved, as also confirmed in the magnet tests [5].

In preparation to the next 0.5 m long undulator model IMM2, the HT schedule was further optimized by reducing the time of the last, highest temperature step of the thermal cycle from 50 h to 40 h, using a dummy coil which included witnesses. The *I* vs. *B* behavior of the most unstable of the latter is also shown in Fig. 6. This time the local minimum of the transport current was 1283 A, i.e. larger than the expected *SSL* of 1205 A (see also Table III). The calculated coil maximum magnetic fields are given in Table IV.

TABLE IV
COIL MAXIMUM FIELDS, T

SMM4	SMM5	SMM6	IMM1	DUMMY
4.98	5.02	5.04	5.26	5.26

B. *Residual Resistivity Ratio (RRR)*

The Residual Resistivity Ratio (*RRR*) was measured as the ratio of the wire resistance at room temperature over its residual resistance at 19 K. The *RRR* averages for witnesses, study and actual coils are shown in Table III and Fig. 7, where the J_c*(12 T, 4.2 K)* are also plotted for each tested sample. RRP1 was a wire with inherently larger *RRR* than RRP2, and there was little difference between the *RRRs* obtained with the

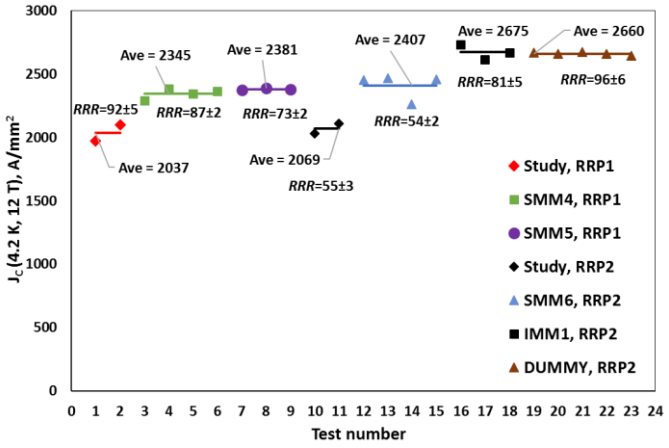

Fig. 7. J_c*(12 T, 4.2 K)* of each tested sample, with average J_c and *RRR* values.

standard HT and those attained with the modified cycle. However, when using the 2 m long oven with larger homogeneity volume for IMM1 and the dummy coil for the modified cycles, not only did the I_c improve by more than 10%, but the *RRR* nearly doubled.

IV. CONCLUSIONS

An ANL APS and the FNAL magnet groups paired forces to develop a double undulator of 2.8 m total length made of Nb_3Sn, to be installed in the APS storage ring. Besides a larger temperature margin than Nb-Ti, Nb_3Sn undulators increase the magnetic field in the electron beam aperture by up to 50%. Of the three phases of this project, the first one was successfully completed. Six short Nb_3Sn models of 4.5 periods length and 10 poles were designed, fabricated and tested.

For short models SMM2 to SMM6, a non-standard heat treatment was used. This heat treatment increased the expected J_c. However, it was important to verify that the selected heat treatment not only provided the best J_c*s*, but also the desired stability in the 5 T region, where the undulator load line intersects the superconductor critical or quench current curve.

The same two RRP wires that were used in the winding of the short magnet models were studied when subjected to the standard heat treatment. Wire I_c and *RRR* were measured and compared with those of the witness samples for SMM4, SMM5, and SMM6, and for intermediate magnet model IMM1 and a dummy coil of same length. It was found that whereas the average I_c*(12 T, 4.2 K)* of the witness samples of the three shorter coils was 16% larger than in the standard heat treatment, their stability was better in the low field region. The non-standard heat treatment was therefore applied also to the first 0.5 m long IMM1 coil in a different, larger furnace. Its witness samples showed an I_c*(12 T, 4.2 K)* nearly 30% larger as well as a *RRR* nearly double. However, the maximum stable transport current at low fields was 90% of the expected *SSL*. The thermal cycle was then further modified using a dummy coil, by shortening the time at the maximum temperature. This produced a similar I_c and *RRR* as for IMM1, and a maximum stable current larger than the *SSL*. The latter optimized thermal cycle was selected for the next undulator coils.

REFERENCES

[1] Y. Ivanyushenkov, K. Harkay et al., "Development and Operating Experience of a Short-Period Superconducting Undulator at the Advanced Photon Source," Phys, Rev. ST Accel. Beams, vol. 18, 2015, p. 040703. doi:10.1103/ PhysRevSTAB.18.040703

[2] Y. Ivanyushenkov et al., "Development and operating experience of a 1.1-m-long superconducting undulator at the Advanced Photon Source," Physical Review Accelerators and Beams, vol. 20, no. 10, 100701, 2017. doi:10.1103/PhysRevAccelBeams.20.100701

[3] M. Kasa et al., "Design, Construction, and Magnetic Field Measurements of a Helical Superconducting Undulator for the Advanced Photon Source," in Proc. IPAC'18, Vancouver, Canada, Apr.-May 2018, pp. 1263-1265. doi:10.18429/JACoW-IPAC2018-TUPMF008

[4] Kesgin et al., "Development of Short-Period Nb_3Sn Superconducting Planar Undulators", IEEE Trans. Appl. Sup., vol. 29 (5), 2019, pp. 1-4.

[5] I. Kesgin et al., "Development of a Nb_3Sn Superconducting Undulator for the Advanced Photon Source," this Conference.

[6] Emanuela Barzi, Alexander V. Zlobin, "Research and Development of Nb_3Sn Wires and Cables for High-Field Accelerator Magnets", IEEE Trans. on Nuclear Science, vol. 63 (2), April 2016, p. 783-803.

[7] Charlie Sanabria et al 2018 Supercond. Sci. Technol. 31 064001.

[8] A.V. Zlobin et al., "Advantages and Challenges of Nb_3Sn Superconducting Planar Undulators," Proceedings of the 9th International Particle Accelerator Conference, Vancouver, BC Canada.

[9] S.O. Prestemon et al., "Design, Fabrication, and Test Results of Undulators Using Nb_3Sn Superconductor," IEEE Trans. on Appl. Supercond., vol. 15 (2), 2005, p. 1236.

[10] S.H. Kim et al., "R&D of short period Nb-Ti and Nb3Sn superconducting undulators for the APS," Proc. of PAC2005, 2005, p. 2419.

[11] H.W. Weijers et al., "A Short-Period High-Field Nb_3Sn Undulator Study," IEEE Trans. on Appl. Supercond., vol. 16 (2), 2006, p. 311.

[12] D.R. Dietderich et al., "Fabrication of a Short-Period Nb_3Sn Superconducting Undulator," IEEE Trans. on Appl. Supercond., vol. 17 (2), 2007, p. 1243.

[13] H.W. Weijers et al., "Assembly Procedures for a Nb_3Sn Undulator Demonstration Magnet," IEEE Trans. on Appl. Supercond., vol. 17 (2), 2007, p. 1239.